Donor Group Influence on Dye-Sensitized Solar Cell Device Performances: Balancing Dye Loading and Donor Size

David Ndaleh D. N., Dinesh Nugegoda, Jonathon Watson, Hammad Cheema, and Jared H. Delcamp*

Department of Chemistry and Biochemistry, University of Mississippi, University, Mississippi 38677, United States

*corresponding author email: delcamp@olemiss.edu

Abstract

Four high photocurrent near-infrared (NIR)-absorbing metal-free organic sensitizers (**ND1**, **ND2**, **ND3**, and **AP25**) with varying nitrogen-based donor groups are examined for use in dye-sensitized solar cell (DSC) devices. One of the highest photocurrent generating organic dyes based on a triarylamine donor reported in the literature (**AP25** at 19 mA/cm^2) is compared to dyes varying the donor group with constant intramolecular charge transfer π-bridge-acceptor systems. Specific popular donor groups include the bulky Hagfeldt donor (**ND1**), a carbazole donor (**ND2**), and an indoline donor (**ND3**) which varies a large range of sizes (maximum width varies between 26 Å and 8 Å). Computational analysis, dye energetics, absorption profiles (in solution and on TiO_2), device incident photon-to-current conversion efficiencies (IPCEs), electrochemical impedance spectroscopy, small modulated photovoltage transient spectroscopy, and device current-voltage curves are used to probe dye behavior based on donor group selection. Balancing donor size and dye loadings was found to be critical for higher performances with the DSC dyes accessing lower energy photons near 900 nm.

Graphical Abstract

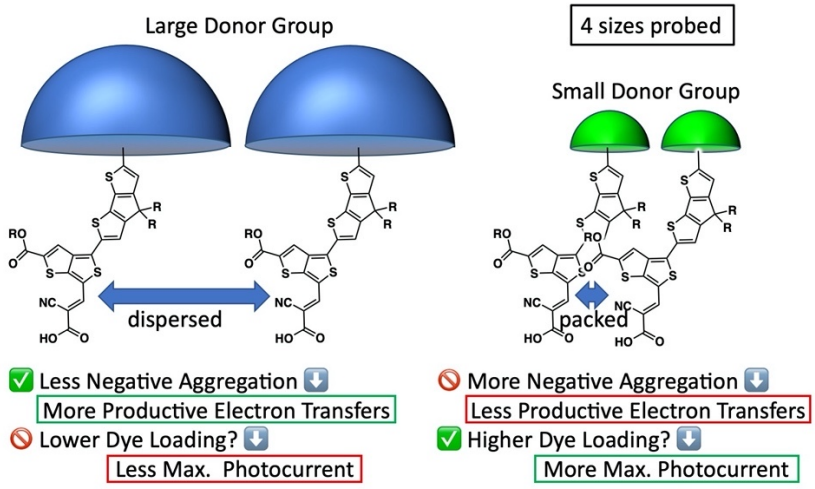

KEYWORDS: dye-sensitized solar cells, photocurrent, insulating groups, donor π-bridge acceptor, sensitizer

INTRODUCTION

Dye-sensitized solar cells (DSCs) have attracted significant attention due to advantages in cost-effective fabrication, high tunability, non-toxic materials, high performance in low-light environments, flexibility, short energy payback time, and efficiency independent of the angle of incident photons.[1-8] In DSC devices, organic sensitizer selection controls the useable photon energy, and dyes using low energy photons are in high demand due to promising theoretical performances.[1] However, organic dyes using low energy photons within DSC devices are scarce in the literature.[9-17] The majority of known organic sensitizers are limited to absorbing higher energy photons in the visible region of the electromagnetic spectrum (approximately ≤750 nm).[2, 5, 7, 18-22] The discovery of photosensitizers absorbing at longer wavelengths is critical to increasing DSC device power conversion efficiencies (PCEs).[1] Accurately understanding dye behavior in solution and on surfaces is critical in the near-infrared (NIR) spectral region where dye energetics must be carefully controlled to maintain favorable electron transfers.[23]

DSC devices function by photoinduced electron transfer processes where a photon is first absorbed by the sensitizer, which then transfers an electron to the conduction band (CB) of a semiconductor (typically TiO_2 for n-type DSCs). The electron then traverses an external circuit where it is collected at a counter electrode by a redox shuttle (RS) which returns the electron to the oxidized dye. Controlling the energetics of the different components (the dye, TiO_2 CB, and the RS) of the device is crucial in the design of an efficient system. To access the NIR region, the free-energy driving force for electron transfers (or overpotential) for each of the electron transfers need to be minimized.[1] Thus, the dye should have energy levels near that of the semiconductor CB and the redox shuttle but maintain favorable free energies of electron

transfer. Among dye designs, the donor-π bridge-acceptor (D-*π*-A) strategy offers flexible dye designs which can be readily tuned to yield desirable dye properties.[22] Specifically, this type of donor-acceptor dye design approach has been critical to accessing NIR photons for use in DSC devices from organic chromophores employing strong electron-donor groups and strong electron-withdrawing groups conjugated through a *π*-bridge.[9-10, 12-13, 24] Additionally, the use of non-conjugated functionality as insulating groups can control dye surface footprint, dye loading densities, dye-dye interactions on the surface of TiO_2 films, and the rate of non-productive recombination of electrons in the TiO_2 CB with an oxidized RS.[22, 25-29]

The size of the respective donor group plays an important role in the performance of the DSC device with current trends favoring bulkier donor designs.[25, 28, 30-34] Amine donors have been widely used in dye design owing to their strong electron donation strength and reversible redox chemistry, allowing localized cations to be held far from the TiO_2 surface and consequently limiting back electron transfers. Among amine donors, one of the most popular donors is the Hagfeldt donor.[30, 35-36] Specifically, this donor and others inspired by its design have sparked continued growth within the DSC field by slowing redox shuttle recombination rates through the use of insulating groups, giving an 'umbrella' effect to the sensitizer and enabling the efficient use of a variety of transition metal based redox shuttles.[30, 37] However, high performances from more concise donor designs such as ethyl-carbazole,[38] indole,[39-42] and bis(4-alkoxyphenyl)aniline derived systems[43-46] have been noted. Additional cases exist where the donor size has modest effects on device performances.[47] Thus studying donor size in general with promising chromophores is an important strategy needed to understand device performances.[26, 34, 48-50] Specifically, for some D-π-A systems, the bulk of the Hagfeldt donor

can lower dye loadings and lead to the diminished performance of the sensitizer compared to more concise donors.[25, 51] With these observations in mind, this study directly compares four of the more commonly used donor groups with an identical π-bridge-acceptor system based on the record setting photocurrent DSC device dye, **AP25**, which was recently used in a 25 mA/cm^2 co-sensitized all organic dye device (Figure 1).[52-53] The Hagfeldt donor (**ND1**), carbazole (**ND2**), indoline (**ND3**) and triarylamine (TAA, **AP25**) donors are compared here based on electron donation strength, dye footprint, dye loading, effects on recombination rates, and overall device performances with the cyclopentadiene (CPDT[44, 54])-3,4-thienothiophene (3,4TT[55])-cyanoacrylic acid (CAA) π-system (Figure 1).

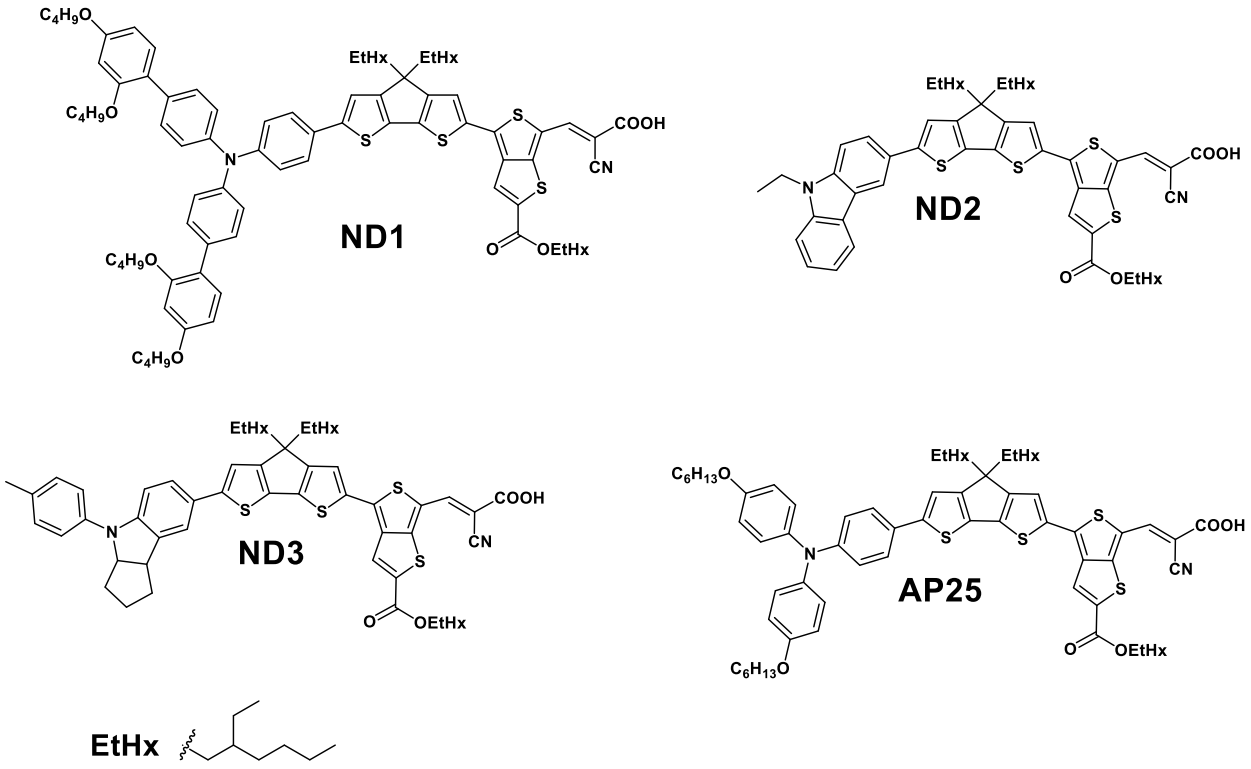

Figure 1. Molecular structures of **ND1**, **ND2**, **ND3**, and **AP25.**

RESULTS AND DISCUSSION

Synthesis of **ND1**, **ND2**, and **ND3** began from a known common brominated CPDT-3,4TT intermediate (**1**) (Scheme 1).[52] Each of the donor group pinacol boronic ester (Bpin) derivatives are either commercially available (Hagfeldt donor, HF-Bpin), or prepared according to reported literature procedures (carbazole donor, Cbz-Bpin[56]; indoline donor, Ind-Bpin[41]). Palladium-catalyzed Suzuki coupling of the pinacol boronic esters of the donor groups yielded aldehyde intermediates **2**-**4** in 43%-78%. A Knoevenagel reaction between **2**-**4** and cyanoacetic acid awarded the target dyes **ND1**-**ND3** in 50%-54% yield. **AP25** with the triarylamine (TAA) donor was prepared according to the literature.[52]

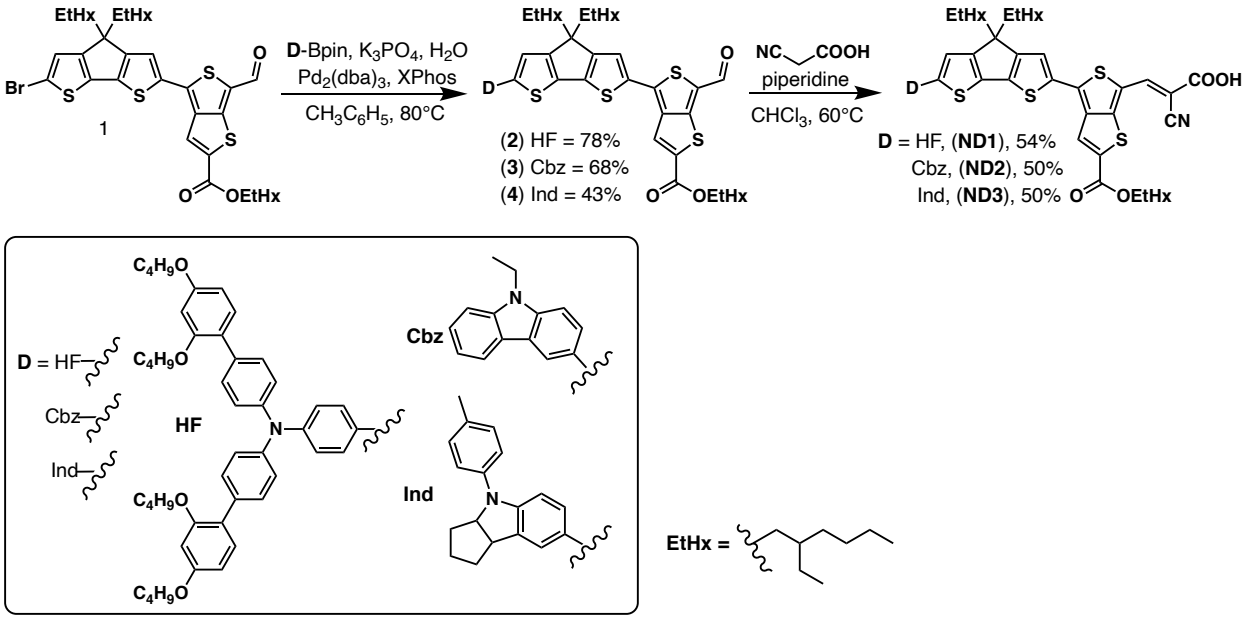

Scheme 1. Synthesis of the target dyes **ND1**, **ND2**, and **ND3.**

Absorption spectroscopy measurements were undertaken with **ND1**, **ND2**, **ND3** and **AP25** both in solution (Figures S1-S2, Table S1) and on the surface of TiO_2 (Figure 2, Table 1) to compare the effect of the donors. The order of increasing absorption maximum (λ_{max}) wavelength values

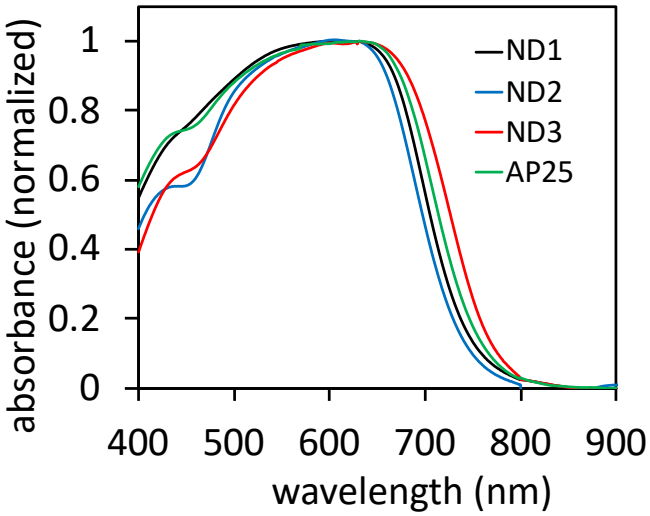

Figure 2: Absorption spectra of **ND1, ND2, ND3** and **AP25** on TiO_2.

Table 1: Energetics of **ND1**, **ND2,** and **ND3**, and **AP25** on TiO_2.

Dye	λ_{max}^{DCM} (nm)	λ_{onset}^{DCM} (nm)	λ_{onset}^{TiO2} (nm)	ε ($M^{-1}cm^{-1}$)	$E_{(S+/S)}^{TiO2}$ (V)	$E_{(S+/S^*)}^{TiO2}$ (V)	$E_g^{opt\ TiO2}$ (eV)
ND1	646	765	755	45000	0.92	-0.72	1.64
ND2	641	735	745	39000	1.00	-0.66	1.66
ND3	668	800	780	42000	0.75	-0.84	1.59
AP25	641	780	765	30000	0.88	-0.74	1.62

of the dyes in dichloromethane (DCM) solution is **ND2** (641 nm) = **AP25** (641 nm) < **ND1** (646 nm) < **ND3** (668 nm) (Figure S1-S2 and Table S1). Notably, the HF, Indz, and TAA donors all have similar λ_{max} energy values within about 5 nm (<0.02 eV). The trend observed for absorption onset (λ_{onset}) in solution does not coincide with the trend observed for λ_{max} since **AP25** has a wider absorption profile than **ND1** and **ND2** (Figure S1). The broad absorption spectra of the dyes reaching near

800 nm is representative of a low energy intramolecular charge transfer (ICT) band. The dyes have molar absorptivities (ε) ranging from 30,000 $M^{-1}cm^{-1}$ to 45,000 $M^{-1}cm^{-1}$ in DCM. **ND1** with the Hagfeldt donor was the strongest absorbing dye in the series (ε = 45,000 $M^{-1}cm^{-1}$) with a similar ε value to **ND2** (ε = 39,000 $M^{-1}cm^{-1}$) and **ND3** (ε = 42,000 $M^{-1}cm^{-1}$). The ε value for **AP25** was notably lower at 30,000 $M^{-1}cm^{-1}$, but the absorption curve was broader.

The optical properties of the organic photosensitizers were analyzed on the TiO_2 surface. While the solution measurements are more easily correlated to structure-function relationships, the surface measurements are more relevant to practical device measurements. On TiO_2 the absorption spectrum broadens dramatically to give a near panchromatic response where the λ_{max} is not easily observed in relation to the lowest energy transition (Figure 2). The λ_{onset} trend is identical to that observed in DCM which suggests the donor strength order increases according to the trend: Cbz < HF < TAA < Ind over a 35 nm range reaching up to 780 nm. Prominent shoulder features are present around 500 nm on TiO_2 which are not present in the solution absorption spectrum which shows a minimum near 500 nm. An additional low energy shoulder near 650-700 nm is also present in the spectrum. The summation of these three transitions (the primary transition and the lower and higher energy shoulders) leads to an apparently panchromatic absorption spectrum across most of the visible region on TiO_2 films.

Cyclic voltammetry (CV) studies were performed to determine the oxidation potentials of the dyes in solution and on the surface of TiO_2 films (Figures S3 and S4, Tables 1 and S1). In DCM, the dyes have ground state oxidation potentials ($E_{(S+/S)}$) ranging from 0.76 V to 0.98 V versus normal hydrogen electrode (NHE) (Table S1). The $E_{(S+/S)}$ value increased in potential according to the following trend: **ND3** < **AP25** < **ND1** < **ND2** indicating that the indoline donor dye has the least

positive oxidation potential and the carbazole donor dye has the most positive potential. The same trend is found when the dyes are bound to TiO_2 with very similar $E_{(S+/S)}$ values observed (≤ 0.07 V difference, Figure 3, Table 1). All of these dyes are well suited for regeneration with the I^-/I_3^- redox shuttle (RS) when on TiO_2 films with driving forces for regeneration (ΔG_{reg}) ranging from 400 mV to 650 mV when oxidation potential of RS is taken at 0.35 V. Notably, this value is a grossly estimated number which is often used in the literature;[6, 20, 57-59] however, the redox chemistry of the RS system is significantly more complex than a single number would indicate.[60-61] The dye excited state oxidation potentials ($E_{(S+/S^*)}$) were found by the following equation: $E_{(S+/S^*)} = E_{(S+/S)} - E_g^{opt}$. The $E_{(S+/S^*)}$ values range from –0.66 V to –0.84 V according to the following trend in order of least to most negative values on TiO_2: **ND2** > **ND1** > **AP25** > **ND3**. Importantly, $E_{(S+/S)}$ and $E_{(S+/S^*)}$ value trends indicate that the donor group choice affects both the ground and excited state oxidation potential values significantly. The dyes have a favorable free-energy driving force for electron injection into the TiO_2 CB of 160 mV to 340 mV when the TiO_2 conduction band is taken at –0.5 V.[19-20, 59, 62]

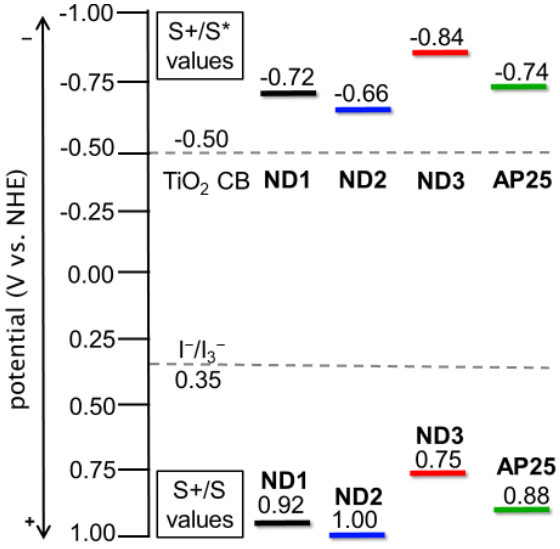

Figure 3: Energetics of **ND1**, **ND2**, **ND3**, and **AP25** on TiO_2.

The highest occupied molecular orbital (HOMO) and lowest unoccupied molecular orbital (LUMO) positions are critically important to directional electron transfer reactions at a TiO_2 surface. The LUMO should be positioned near TiO_2 for efficient electron injection from the photoexcited dye to the TiO_2 semiconductor. The HOMO should be located away from the TiO_2 semiconductor to avoid back electron transfer from the semiconductor to the oxidized dye after the initial photoinduced charge separation event occurs. Density functional theory (DFT) and time dependent (TD)-DFT calculations were carried out at the B3LYP[63-64]/6-311G(d,p)[65] level with the Gaussian16 package[66] to assess the HOMO and LUMO locations on the dyes (Figure 4). The HOMO was found to be delocalized across the donor

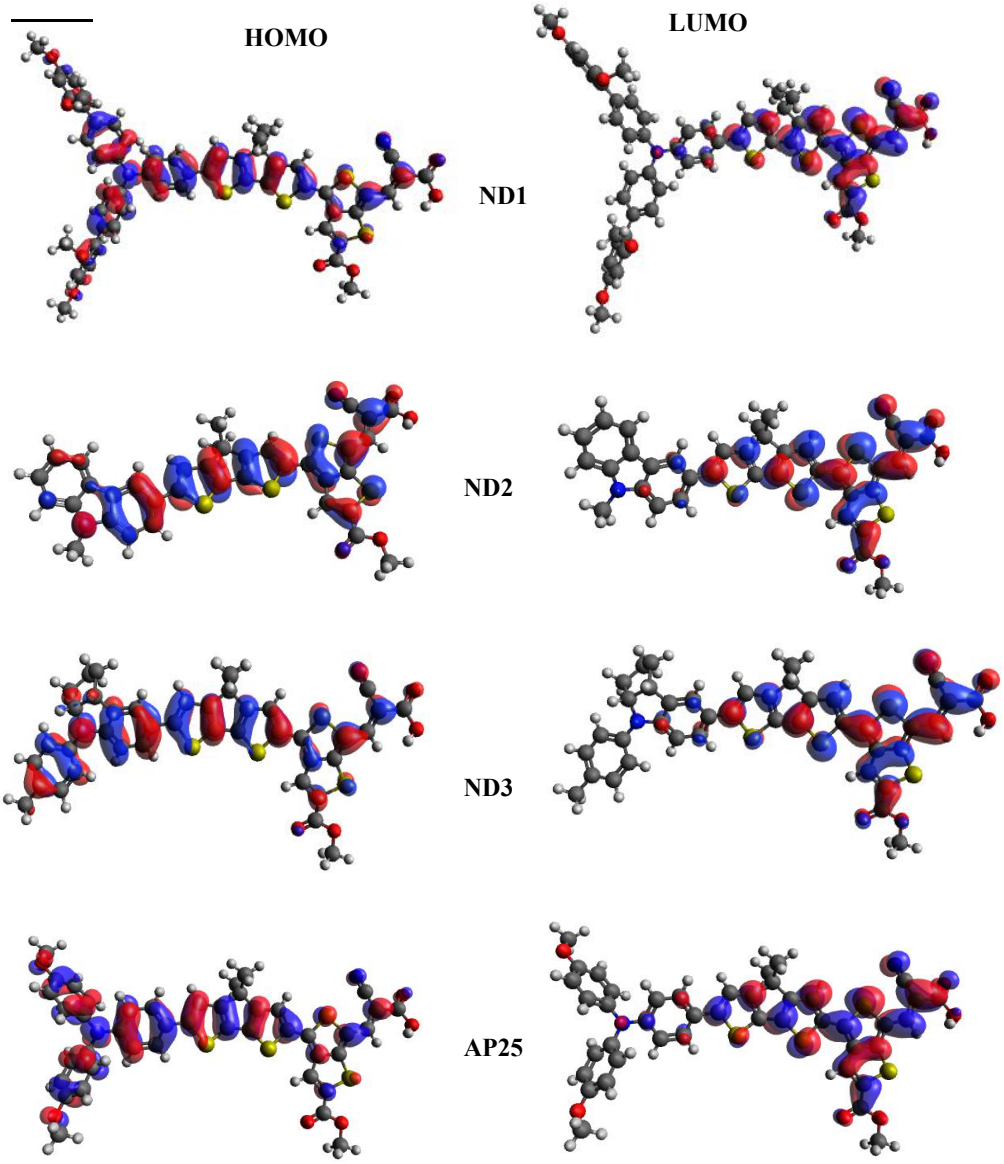

Figure 4. Frontier orbital distribution of **ND1**, **ND2**, **ND3** and **AP25** at the B3LYP/6311(d,p) level of theory. Iso values set to 0.02.

and the π-bridge with a small presence on the acceptor region in each of the dyes. The LUMO was delocalized from the CPDT π-bridge across the 3,4TT group and onto the cyanoacrylic acid acceptor group with each dye. The presence of the LUMO on the dye anchoring group allows for facile electron transfer from the dye to TiO_2. This HOMO is mostly positioned away from the TiO_2 surface by the acceptor region to slow back electron transfer processes after photoinduced

charge separation. After electron transfer to TiO_2 and dye geometry reorganization, the dye cation singly occupied molecular orbital (SOMO) position is important for sustained charge separation. Additionally, the dye cation geometries were optimized, and the SOMO was found to be delocalized primarily from the donor group across the π-bridge with some contribution also on the acceptor (Figure S7). This illustrates a very broad delocalization of the SOMO orbital of the dye cations with some undesirable proximity to the TiO_2 surface. Notably, the positions of both the HOMO and LUMO suggest these dyes are behaving as intramolecular charge transfer (ICT) dyes with orbital overlap on the π-bridges. Time dependent-DFT reveals the HOMO and LUMO orbitals contribute >99% to the S_0 to S_1 transition with high oscillator strengths above 1 (Table S2). Thus, based on orbital analysis, electrochemical, and optical properties, these dyes are well-suited for DSC device studies.

DSC devices were fabricated with **ND1**, **ND2**, **ND3** and **AP25**. An AM 1.5G solar simulated spectrum at 1 sun intensity was used as a light source to measure the device performances via current-voltage (J-V) curve measurements (Figure 5, Table 2). The power conversion efficiency (PCE) of the cells was calculated according to the equation $PCE = (J_{sc} \times V_{oc} \times FF)/I_0$, where J_{sc} is the short-circuit current density, V_{oc} is the open-circuit voltage, FF is the fill factor, and I is the incident light intensity equal to 1 sun (1000 W/m^2).

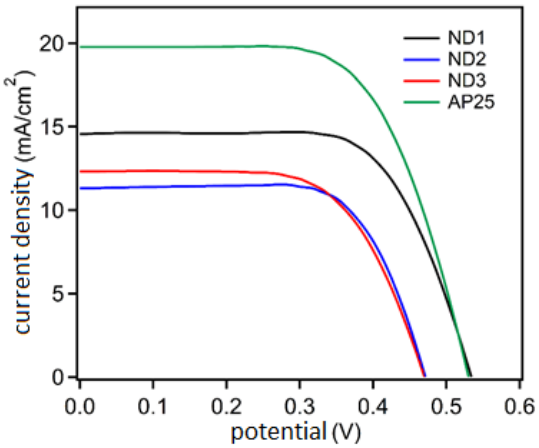

Figure 5: *J-V* curve for **ND1, ND2,** and **ND3** compared to **AP25.**

The DSC devices produce photocurrents ranging from 11.7 mA/cm^2 to 19.1 mA/cm^2 for each of the single dye devices according to the following trend: **ND3** ≅ **ND2** < **ND1** < **AP25** (Table 2, Figure 5). Thus, the TAA donor led to the highest photocurrent followed by the HF donor dye and then the carbazole and indoline dyes. Since all of the dyes have very similar absorption onset values, addition studies are show below to help understand this trend. The photovoltage trend was similar to the photocurrent trend with **ND2** < **ND3** < **AP25** < **ND1** ranging from 477 mV to 544 mV. The modest photovoltage values are due to using high lithium iodide loading to facilitate facile electron transfers which is necessary as has been previously reported for **AP25** and is apparent from devices fabricated without LiI (Figure S10, Table S5).[52] Additionally, dipole moments at the TiO_2 surface are known to have significant effects on the photovoltages of DSC devices.[67] The dipole values are similar debye amounts for the dyes studied here (~14 D neutral dye, 16-19 D cationic dye) which are correlated in the literature to low photovoltage (Tables S2-S3).[24] The devices show similar FF values and an overall PCE range of 3.7% to 6.7%. However, given the high photocurrent and broad absorptions of these dyes, they are interesting candidates

for multijunction solar cell devices despite the modest PCE values.[52-53] Additionally, these broadly absorbing dyes are excellent for pairing with wider energy gap dyes like **D35** for a co-sensitized device.[6, 36, 68-69] The overall PCE and photocurrents of both **AP25** and **ND1** were substantially improved by co-sensitization with **D35** resulting in the improvement of photocurrent production in the visible region near 400 nm for the two single dye devices as demonstrated in their respective incident photon-to-current conversion efficiency (IPCE) spectra (Figure 6, IPCE discussion below). This results in an increase of near 4 mA/cm^2 of photocurrent and an increase in PCE from 5.3% to 7.3% with **ND1**.

Table 2. Current-voltage curve data for the DSC devices**.**

Device	V_{oc} (mV)	J_{sc} (mA/cm^2)	FF (%)	PCE (%)	dye loading (mol/cm^2)
ND1	541 ± 9	14.5 ± 0.6	67 ± 0	5.3 ± 0.1	1.02×10^{-7}
ND2	477 ± 3	11.7 ± 0.3	69 ± 0	3.7 ± 0.1	1.06×10^{-7}
ND3	498 ± 5	11.8 ± 0.2	65 ± 0	3.8 ± 0.1	1.23×10^{-7}
AP25	530 ± 2	19.1 ± 0.7	66 ± 0	6.7 ± 0.1	1.54×10^{-7}
ND1+D35	572 ± 6	18.1 ± 0.1	71 ± 1	7.3 ± 0.3	
AP25+D35	570 ± 11	23.7 ± 0.7	63 ± 1	8.3 ± 0.2	

*Values are the average of at a least two DSC devices.

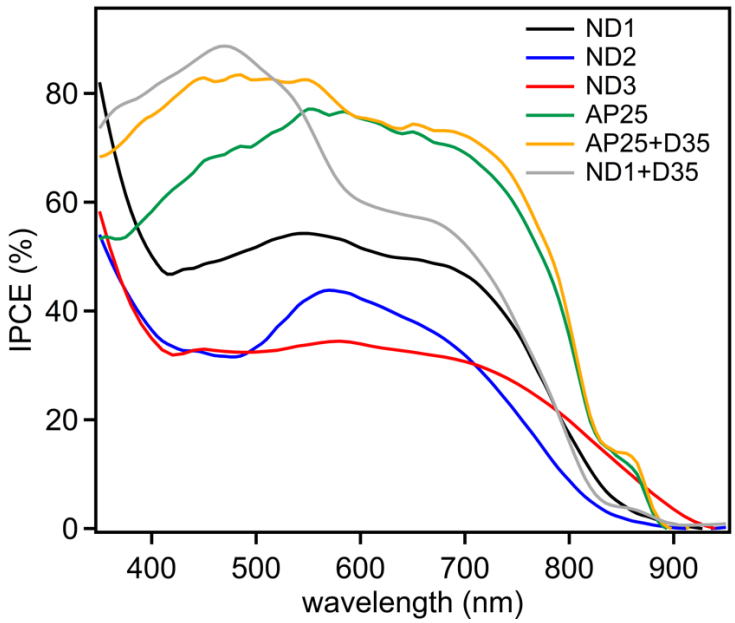

Figure 6: IPCE spectra of **ND1, ND2, ND3** and **AP25** based DSC devices**.**

Incident photon-to-current conversion efficiency (IPCE) measurements were taken to better understand the photocurrent trend observed during current-voltage curve measurements. The IPCE onset values for all of the dyes is similar at ~900 nm. However, the peak IPCE value in the 400-900 nm region varies dramatically for the series of dyes and correlates with the photocurrent values measured for the DSC devices with a <1 mA/cm^2 difference between the IPCE integrated current area and that obtained by *J-V* curve measurements. The peak IPCE values gave the following trend: **AP25** (TAA donor, ~80%) > **ND1** (HF donor, 55%) > **ND2** (Cbz donor, 45%) > **ND3** (Ind donor, 35%). This trend is similar to that observed for photocurrent measurements from the J-V curves except for **ND3** being lower in peak IPCE value despite a slightly higher J_{SC} value than **ND2**. However, **ND3** produces electricity at a higher level further into the long wavelength region of the IPCE spectrum leading to a higher photocurrent than **ND2**. The low IPCE value of **ND2** is attributed to a small free energy of electron injection (ΔG_{inj}) for

photoinduced electron transfer from the dye to TiO_2 at only 160 mV (Figure S6). The low IPCE value for **ND3** is attributed to a low driving force for dye regeneration (ΔG_{reg}) with the I^-/I_3^- redox shuttle of only 400 mV when ≥550 mV is commonly needed for efficient regeneration (Figure S6).[60]

Dye loading studies were undertaken to evaluate the effect of each donor on the amount of dye deposited on the TiO_2 electrode. The highest dye loading was obtained with the TAA dye **AP25** at 1.54 x 10^{-7} mol/cm^2. The remaining dyes follow the trend: **ND3** (1.23 x 10^{-7} mol/cm^2) > **ND2** (1.06 x 10^{-7} mol/cm^2) > **ND1** (1.02 x 10^{-7} mol/cm^2) (Table 2). The dye loading trend is different to the simplified trend often analyzed computationally for the donor diameters which were measured to be between 8.4 Å and 26.4 Å as follows: **ND2** (8.3 Å) < **ND3** (10.3 Å) < **AP25** (25.0 Å) < **ND1** (26.4 Å) (Figure S11). Notably, these two measurements do not need to correlate since the dye-dye packing, dye orientation, and aggregation events can all perturb dye loading values but are not accounted for in the donor size computational analysis. Given that **ND1** has a 33% lower dye loading than **AP25** this can account for the relatively higher peak IPCE value of **AP25**. Fabrication of DSC devices with an additional 5 µm TiO_2 active layer thickness with **ND1** led to a a 16.5 mA/cm^2 device (6.3% PCE) which illustrates the low loading of **ND1** limiting light absorption to be a primary factor when **AP25** and **ND1** are compared at typical 10 µm TiO_2 thicknesses.

Small modulated photovoltage transient (SMPVT) measurements were undertaken to better understand how the donor perturbs the charge separation lifetime which is a measure of the recombination rate of electrons in TiO_2 with the electrolyte as a function of applied light intensity (Figure 7).[70-71] The electron lifetime

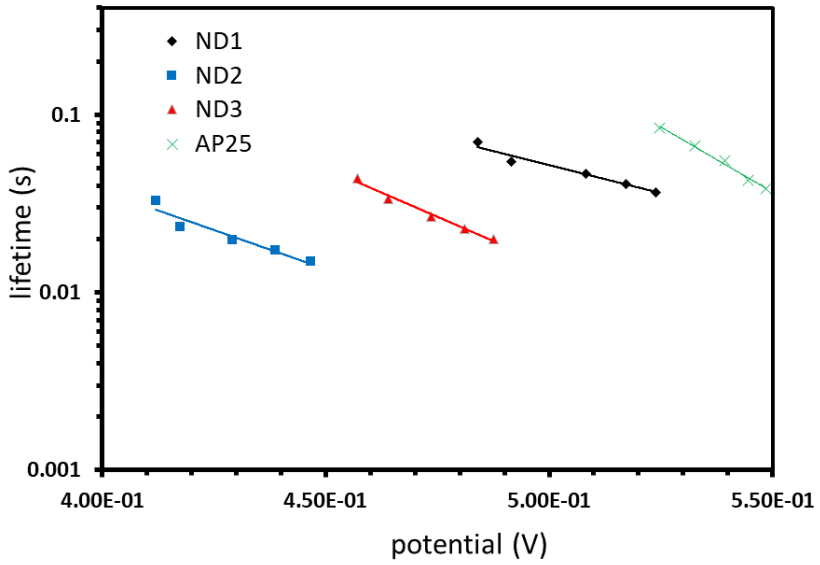

Figure 7: Small modulated photovoltage transient electron lifetime in TiO_2 for **ND1**, **ND2**, **ND3**, and **AP25** based devices**.**

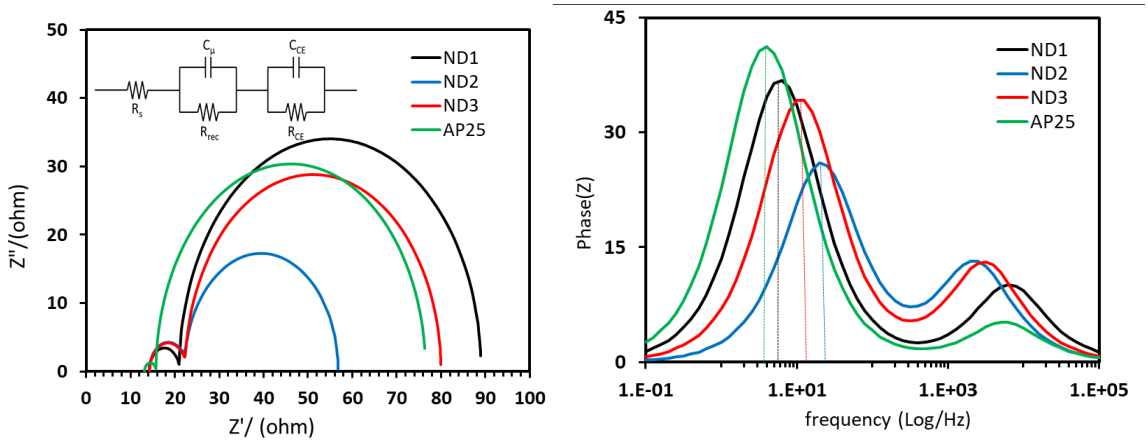

Figure 8: Nyquist Plot (left) and Bode plot (right) of **ND1**, **ND2**, **ND3**, and **AP25**.

in TiO_2 of the devices follows the order **AP25** > **ND1** > **ND3** > **ND2**. Electrochemical impedance spectroscopy (EIS) experiments were also conducted on each of the dyes at open-circuit potential bias to probe electron transfer resistances and electron lifetimes via a second technique in the dark (Figure 8, Table S4). EIS studies with the Bode plot (Figure 8) show an identical electron lifetime in TiO_2 trend to that observed with SMPVT. The low frequency peak value (f) of each

curve on the Bode plot is related to the electron lifetime in TiO_2 through the formula $\tau_{TiO2} = 1/(2\pi f)$. Furthermore, analysis of the Nyquist plot shows that charge recombination resistance (R_{rec}) across the TiO_2-dye-electrolyte interface (large semi-circle) is smallest for the **ND2** devices and largest for **AP25** and **ND1** based devices (Figure 8, Table S2). Charge collection efficiency (η_{cc}) is calculated via the equation, $\eta_{cc} = 1/(1 + (R_{CE}/R_{rec}))$, where R_{CE} is the electron transfer resistance at the counter electrode-electrolyte interface (the smaller semi-circle) and is small (<10 Ω) in all cases. Notably, the devices all have good η_{cc} values that range from 81% to 96% (Table S4).

The trend in electron lifetimes observed by both SMPVT and EIS measurements is a result of the balance of donor size versus dye loading amounts. While **AP25** has the second largest donor (5% smaller than **ND1**), **AP25** does have the highest dye loading (33% more than **ND1**) which leads to a higher coverage of the TiO_2 surface than the larger donor **ND1** dye. This example shows a case where dye loading was a more important factor for surface coverage than donor size. The opposite observation is made when **ND3** and **ND1** are compared. **ND3** has a 17% higher dye loading than **ND1**, but is a substantially smaller donor (61% smaller) which leads to a better surface protection from **ND1**. Thus, the balance between dye loading and donor size is critical to accessing the highest performing system, and should be studied for promising chromophores.

Conclusion

Four metal-free organic sensitizers absorbing into the NIR region of the electromagnetic spectrum were compared to study the effect of varying the nitrogen-based donor group through

the use of the Hagfeldt, carbazole, indoline and triarylamine donors. Dye energetics and the effects of the donor groups on the behavior of the dyes were probed via absorption spectroscopy and cyclic voltammetry (in solution and on TiO_2). The donor groups were found to have a significant influence on both the ground and excited state energies. Computational studies reveal that all of the dyes are intramolecular charge transfer systems upon photoexcitation with orbitals well positioned for facile photoinduced interfacial charge separation at TiO_2. Dye-sensitized solar cell devices were studies through current-voltage curves, incident photon-to-current conversion efficiencies (IPCEs), small modulated photovoltage transient spectroscopy, electrochemical impedance spectroscopy, and dye loading density studies. These results show that a balance between donor size and dye loading must be reached for optimal performance in this system. An examples is presented where the donor group is large but the dye loading is lower leading to a lower performing system. Conversely, a case is presented where the dye loading is higher but the donor group is small which also leads to a lower performing system. These results may explain the popularity of the triarylamine in my dye-sensitized systems despite the known benefits of bulky donors if high dye loadings can be achieved.[30] This work highlights the necessary evaluation of donors of similar electron donation strengths with new chromophores for dye-sensitized applications since the dye loading is contingent on a number of difficult to predict factors. Future studies on this chromophore system are planned since it has shown on of the highest photocurrent systems known in the DSC literature with relatively deep NIR photon use for the DSC field. Continued studies in this spectral region are critical to improving many applications including multi-junction solar cell systems that work in harmony with existing high performing solar cell technologies.

Acknowledgments

This work was supported by the National Science Foundation (NSF 1954922). Preliminary data was collected under NSF 1455167.

References

[1] Hardin BE, Snaith HJ, McGehee MD. The renaissance of dye-sensitized solar cells. Nat. Photon. 2012;6,162-9.

[2] Zhang S, Yang X, Numata Y, Han L. Highly efficient dye-sensitized solar cells: Progress and future challenges. Energy Environ. Sci. 2013;6,1443-64.

[3] Fakharuddin A, Jose R, Brown TM, Fabregat-Santiago F, Bisquert J. A perspective on the production of dye-sensitized solar modules. Energy Environ. Sci. 2014;7,3952-81.

[4] Polman A, Knight M, Garnett EC, Ehrler B, Sinke WC. Photovoltaic materials: Present efficiencies and future challenges. Science 2016;352,aad4424.

[5] Saifullah M, Gwak J, Yun JH. Comprehensive review on material requirements, present status, and future prospects for building-integrated semitransparent photovoltaics (BISTPV). J. Mater. Chem. A 2016;4,8512-40.

[6] Cole JM, Pepe G, Al Bahri OK, Cooper CB. Cosensitization in dye-sensitized solar cells. Chem. Rev. 2019;119,7279-327.

[7] Nam S-H, Lee KH, Yu J-H, Boo J-H. Review of the development of dyes for dye-sensitized solar cells. Applied Science and Convergence Technology 2019;28,194-206.

[8] Huaulmé Q, Mwalukuku VM, Joly D, Liotier J, Kervella Y, Maldivi P, et al. Photochromic dye-sensitized solar cells with light-driven adjustable optical transmission and power conversion efficiency. Nature Energy 2020.

[9] Brogdon P, Cheema H, Delcamp JH. Near-infrared-absorbing metal-free organic, porphyrin, and phthalocyanine sensitizers for panchromatic dye-sensitized solar cells. ChemSusChem 2018;11,86-103.

[10] Shen Z, Chen J, Li X, Li X, Zhou Y, Yu Y, et al. Synthesis and photovoltaic properties of powerful electron-donating indeno[1, 2-b]thiophene-based green D–A−π–A sensitizers for dye-sensitized solar cells. ACS Sustainable Chem. Eng. 2016;4,3518-25.

[11] Qin C, Numata Y, Zhang S, Yang X, Islam A, Zhang K, et al. Novel near-infrared squaraine sensitizers for stable and efficient dye-sensitized solar cells. Adv. Funct. Mater. 2014;24,3059-66.

[12] Eom YK, Kang SH, Choi IT, Yoo Y, Kim J, Kim HK. Significant light absorption enhancement by a single heterocyclic unit change in the π-bridge moiety from thieno[3,2-b]benzothiophene to thieno[3,2-b]indole for high performance dye-sensitized and tandem solar cells. J. Mater. Chem. A 2017;5,2297-308.

[13] Li J-Y, Chen C-Y, Ho W-C, Chen S-H, Wu C-G. Unsymmetrical squaraines incorporating quinoline for near infrared responsive dye-sensitized solar cells. Org. Lett. 2012;14,5420-3.

[14] Ball JM, Davis NKS, Wilkinson JD, Kirkpatrick J, Teuscher J, Gunning R, et al. A panchromatic anthracene-fused porphyrin sensitizer for dye-sensitized solar cells. RSC Adv. 2012;2.

[15] Liu Y, Lin H, Li J, Dy JT, Tamaki K, Nakazaki J, et al. Ethynyl-linked push-pull porphyrin hetero-dimers for near-IR dye-sensitized solar cells: Photovoltaic performances versus excited-state dynamics. Phys Chem Chem Phys 2012;14,16703-12.

[16] Cheema H, Baumann A, Loya EK, Brogdon P, McNamara LE, Carpenter CA, et al. Near-infrared-absorbing indolizine-porphyrin push-pull dye for dye-sensitized solar cells. ACS Appl Mater Interfaces 2019;11,16474-89.

[17] Liu Y, Lin H, Dy JT, Tamaki K, Nakazaki J, Nakayama D, et al. N-fused carbazole-zinc porphyrin-free-base porphyrin triad for efficient near-IR dye-sensitized solar cells. Chem. Commun. 2011;47,4010-2.

[18] Wu Y, Zhu WH, Zakeeruddin SM, Gratzel M. Insight into D-A-π-A structured sensitizers: A promising route to highly efficient and stable dye-sensitized solar cells. ACS Appl. Mater. Interfaces 2015;7,9307-18.

[19] Mishra A, Fischer MK, Bauerle P. Metal-free organic dyes for dye-sensitized solar cells: From structure: Property relationships to design rules. Angew. Chem. Int. Ed. 2009;48,2474-99.
[20] Hagfeldt A, Boschloo G, Sun L, Kloo L, Pettersson H. Dye-sensitized solar cells. Chem. Rev. 2010;110,6595-663.
[21] Ahmad S, Guillén E, Kavan L, Grätzel M, Nazeeruddin MK. Metal free sensitizer and catalyst for dye sensitized solar cells. Energy Environ. Sci. 2013;6,3439-66.
[22] Ji J-M, Zhou H, Kim HK. Rational design criteria for D-π-A structured organic and porphyrin sensitizers for highly efficient dye-sensitized solar cells. J. Mater. Chem. A 2018;6,14518-45.
[23] Peddapuram A, Cheema H, McNamara L, Zhang Y, Hammer N, Delcamp J. Quinoxaline-based dual donor, dual acceptor organic dyes for dye-sensitized solar cells. Applied Sciences 2018;8,1421.
[24] Aumaitre C, Rodriguez-Seco C, Jover J, Bardagot O, Caffy F, Kervella Y, et al. Visible and near-infrared organic photosensitizers comprising isoindigo derivatives as chromophores: Synthesis, optoelectronic properties and factors limiting their efficiency in dye solar cells. J. Mater. Chem. A 2018;6,10074-84.
[25] Liyanage NP, Cheema H, Baumann AR, Zylstra AR, Delcamp JH. Effect of donor strength and bulk on thieno[3,4-b]-pyrazine-based panchromatic dyes in dye-sensitized solar cells. ChemSusChem 2017;10,2635-41.
[26] Huckaba AJ, Yella A, Brogdon P, Scott Murphy J, Nazeeruddin MK, Grätzel M, et al. A low recombination rate indolizine sensitizer for dye-sensitized solar cells. Chem. Commun. 2016;52,8424-7.
[27] Alagumalai A, Mk MF, Vellimalai P, Sil MC, Nithyanandhan J. Effect of out-of-plane alkyl group's position in dye sensitized solar cell efficiency: A structure-property relationship utilizing indoline based unsymmetrical squaraine dyes. ACS Appl. Mater. Interfaces 2016;8,35353-67.
[28] Sanchez Carballo M, Urbani M, Chandiran AK, Gonzalez-Rodriguez D, Vazquez P, Gratzel M, et al. Branched and bulky substituted ruthenium sensitizers for dye-sensitized solar cells. Dalton. Trans. 2014;43,15085-91.
[29] Wu KL, Huckaba AJ, Clifford JN, Yang YW, Yella A, Palomares E, et al. Molecularly engineered Ru(II) sensitizers compatible with cobalt(II/III) redox mediators for dye-sensitized solar cells. Inorg. Chem. 2016;55,7388-95.
[30] Baumann A, Curiac C, Delcamp JH. The hagfeldt donor and use of next-generation bulky donor designs in dye-sensitized solar cells. ChemSusChem 2020;13,2503-12.
[31] Kono T, Masaki N, Nishikawa M, Tamura R, Matsuzaki H, Kimura M, et al. Interfacial charge transfer in dye-sensitized solar cells using scn-free terpyridine-coordinated Ru complex dye and co complex redox couples. ACS Appl Mater Interfaces 2016;8,16677-83.
[32] Higashino T, Kawamoto K, Sugiura K, Fujimori Y, Tsuji Y, Kurotobi K, et al. Effects of bulky substituents of push–pull porphyrins on photovoltaic properties of dye-sensitized solar cells. ACS Appl. Mater. Interfaces 2016;8,15379-90.
[33] Ragoussi ME, Yum JH, Chandiran AK, Ince M, de la Torre G, Gratzel M, et al. Sterically hindered phthalocyanines for dye-sensitized solar cells: Influence of the distance between the aromatic core and the anchoring group. ChemPhysChem 2014;15,1033-6.
[34] Yang J, Ganesan P, Teuscher J, Moehl T, Kim YJ, Yi C, et al. Influence of the donor size in D-π-A organic dyes for dye-sensitized solar cells. J. Am. Chem. Soc. 2014;136,5722-30.
[35] Baumann A, Watson J, Delcamp JH. Robust, scalable synthesis of the bulky hagfeldt donor for dye-sensitized solar cells. ChemSusChem 2020;13,283-6.
[36] Feldt SM, Gibson EA, Gabrielsson E, Sun L, Boschloo G, Hagfeldt A. Design of organic dyes and cobalt polypyridine redox mediators for high-efficiency dye-sensitized solar cells. J. Am. Chem. Soc. 2010;132,16714-24.

[37] Saygili Y, Stojanovic M, Flores-Díaz N, Zakeeruddin SM, Vlachopoulos N, Grätzel M, et al. Metal coordination complexes as redox mediators in regenerative dye-sensitized solar cells. Inorganics 2019;7,30.
[38] Kakiage K, Aoyama Y, Yano T, Oya K, Fujisawa JI, Hanaya M. Highly-efficient dye-sensitized solar cells with collaborative sensitization by silyl-anchor and carboxy-anchor dyes. Chem. Commun. 2015;51,15894-7.
[39] Xie Y, Wu W, Zhu H, Liu J, Zhang W, Tian H, et al. Unprecedentedly targeted customization of molecular energy levels with auxiliary-groups in organic solar cell sensitizers. Chem. Sci. 2016;7,544-9.
[40] Ito S, Miura H, Uchida S, Takata M, Sumioka K, Liska P, et al. High-conversion-efficiency organic dye-sensitized solar cells with a novel indoline dye. Chem. Commun. 2008,5194-6.
[41] Brogdon P, Giordano F, Puneky GA, Dass A, Zakeeruddin SM, Nazeeruddin MK, et al. A computational and experimental study of thieno[3,4-b]thiophene as a proaromatic π-bridge in dye-sensitized solar cells. Chem. Eur. J. 2016;22,694-703.
[42] Zhang W, Wu Y, Li X, Li E, Song X, Jiang H, et al. Molecular engineering and sequential cosensitization for preventing the "trade-off" effect with photovoltaic enhancement. Chem Sci 2017;8,2115-24.
[43] Ren Y, Sun D, Cao Y, Tsao HN, Yuan Y, Zakeeruddin SM, et al. A stable blue photosensitizer for color palette of dye-sensitized solar cells reaching 12.6% efficiency. J. Am. Chem. Soc. 2018;140,2405-8.
[44] Zhang M, Wang Y, Xu M, Ma W, Li R, Wang P. Design of high-efficiency organic dyes for titania solar cells based on the chromophoric core of cyclopentadithiophene-benzothiadiazole. Energy Environ. Sci. 2013;6,2944-9.
[45] Wang P, Yang L, Wu H, Cao Y, Zhang J, Xu N, et al. Stable and efficient organic dye-sensitized solar cell based on ionic liquid electrolyte. Joule 2018;2,2145-53.
[46] Wang J, Liu K, Ma L, Zhan X. Triarylamine: Versatile platform for organic, dye-sensitized, and perovskite solar cells. Chem. Rev. 2016;116,14675-725.
[47] Tang Y, Wang Y, Li X, Agren H, Zhu WH, Xie Y. Porphyrins containing a triphenylamine donor and up to eight alkoxy chains for dye-sensitized solar cells: A high efficiency of 10.9%. ACS Appl. Mater. Interfaces 2015;7,27976-85.
[48] Zhang X, Mao J, Wang D, Li X, Yang J, Shen Z, et al. Comparative study on pyrido[3,4-b]pyrazine-based sensitizers by tuning bulky donors for dye-sensitized solar cells. ACS Appl. Mater. Interfaces 2015;7,2760-71.
[49] Seo KD, Choi IT, Kim HK. D–π–A organic dyes with various bulky amine-typed donor moieties for dye-sensitized solar cells employing the cobalt electrolyte. Org. Electron. 2015;25,1-5.
[50] Wang Z, Wang H, Liang M, Tan Y, Cheng F, Sun Z, et al. Judicious design of indoline chromophores for high-efficiency iodine-free dye-sensitized solar cells. ACS Appl. Mater. Interfaces 2014;6,5768-78.
[51] Cheema H, Peddapuram A, Adams RE, McNamara LE, Hunt LA, Le N, et al. Molecular engineering of NIR absorbing thienopyrazine double donor double acceptor organic dyes for DSCs. J. Org. Chem. 2017;82,12038-49.
[52] Cheema H, Watson J, Peddapuram A, Delcamp JH. A 25 mA cm^{-2} dye-sensitized solar cell based on a near-infrared-absorbing organic dye and application of the device in SSM-DSCs. Chem. Commun. 2020;56,1741-4.
[53] Cheema H, Watson J, Shinde PS, Rodrigues RR, Pan S, Delcamp JH. Precious metal-free solar-to-fuel generation: SSM-DSCs powering water splitting with nanocot and nimozn electrocatalysts. Chem. Commun. 2020;56,1569-72.

[54] Hu Y, Abate A, Cao Y, Ivaturi A, Zakeeruddin SM, Grätzel M, et al. High absorption coefficient cyclopentadithiophene donor-free dyes for liquid and solid-state dye-sensitized solar cells. J. Phys. Chem. C 2016;120,15027-34.
[55] Chen YC, Chou HH, Tsai MC, Chen SY, Lin JT, Yao CF, et al. Thieno[3,4-b]thiophene-based organic dyes for dye-sensitized solar cells. Chem. Eur. J. 2012;18,5430-7.
[56] Xue P, Sun J, Chen P, Gong P, Yao B, Zhang Z, et al. Strong solid emission and mechanofluorochromism of carbazole-based terephthalate derivatives adjusted by alkyl chains. J. Mater. Chem. C 2015;3,4086-92.
[57] Sun Z, Liang M, Chen J. Kinetics of iodine-free redox shuttles in dye-sensitized solar cells: Interfacial recombination and dye regeneration. Acc. Chem. Res. 2015;48,1541-50.
[58] Pashaei B, Shahroosvand H, Abbasi P. Transition metal complex redox shuttles for dye-sensitized solar cells. RSC Adv. 2015;5,94814-48.
[59] Anderson AY, Barnes PRF, Durrant JR, O'Regan BC. Quantifying regeneration in dye-sensitized solar cells. J. Phys. Chem. C 2011;115,2439-47.
[60] Boschloo G, Hagfeldt A. Characteristics of the iodide/triiodide redox mediator in dye-sensitized solar cells. Acc. Chem. Res. 2009;42,1819-26.
[61] Ardo S, Meyer GJ. Photodriven heterogeneous charge transfer with transition-metal compounds anchored to TiO_2 semiconductor surfaces. Chem. Soc. Rev. 2009;38,115-64.
[62] Urbani M, Grätzel M, Nazeeruddin MK, Torres T. Meso-substituted porphyrins for dye-sensitized solar cells. Chem. Rev. 2014;114,12330-96.
[63] Becke AD. Density-functional thermochemistry. III. The role of exact exchange. J. Chem. Phys. 1993;98,5648-52.
[64] Lee C, Yang W, Parr RG. Development of the Colle-Salvetti correlation-energy formula into a functional of the electron density. Physical Review B 1988;37,785-9.
[65] Frisch MJ, Pople JA, Binkley JS. Self-consistent molecular orbital methods 25. Supplementary functions for gaussian basis sets. J Chem Phys 1983;80,3265-9.
[66] Frisch MJ, Trucks GW, Schlegel HB, Scuseria GE, Robb MA, Cheeseman JR, et al. Gaussian 16, Revision A.03 2016,Gaussian, Inc., Wallingford CT.
[67] Rühle S, Greenshtein M, Chen S-G, Merson A, PIzem H, Sukenik CS, et al. Molecular adjustment of the electronic properties of nanoporous electrodes in dye-sensitized solar cells. J. Phys. Chem. B 2005;109,18907-13.
[68] Gabrielsson E, Ellis H, Feldt S, Tian H, Boschloo G, Hagfeldt A, et al. Convergent/divergent synthesis of a linker-varied series of dyes for dye-sensitized solar cells based on the D35 donor. Adv. Energy Mater. 2013;3,1647-56.
[69] Peddapuram A, Cheema H, Adams RE, Schmehl RH, Delcamp JH. A stable panchromatic green dual acceptor, dual donor organic dye for dye-sensitized solar cells. J. Phys. Chem. C 2017;121,8770-80.
[70] Boschloo G, Häggman L, Hagfeldt A. Quantification of the effect of 4-tert-butylpyridine addition to I^-/I_3^- redox electrolytes in dye-sensitized nanostructured TiO_2 solar cells. J. Phys. Chem. B 2006;110,13144-50.
[71] Nissfolk J, Fredin K, Hagfeldt A, Boschloo G. Recombination and transport processes in dye-sensitized solar cells invetigated under working conditions. J. Phys. Chem. B 2006;110,17715-8.